


On the chances and challenges of combining electron-collecting *n*POLO and hole-collecting Al-*p*⁺ contacts in highly efficient *p*-type c-Si solar cells

Robby Peibst^{1,2}  | Felix Haase² | Byungsul Min² | Christina Hollemann² | Till Brendemühl² | Karsten Bothe² | Rolf Brendel^{2,3}

¹Institute of Electronic Materials and Devices, Leibniz Universität Hannover, Hannover, Germany

²Institute for Solar Energy Research Hamelin (ISFH), Emmerthal, Germany

³Department of Solar Energy, Institute for Solid-State Physics, Leibniz Universität Hannover, Hannover, Germany

Correspondence

Robby Peibst, Institute for Solar Energy Research Hamelin (ISFH), Am Ohrberg 1, 31860 Emmerthal, Germany.
Email: r.peibst@isfh.de

Funding information

Federal Ministry for Economic Affairs and Energy, Grant/Award Numbers: 03EE1012A, 0324275A; Leibniz University Hannover

Abstract

ISFH is following a distinct cell development roadmap, which comprises—as a short-term concept—the combination of an *n*-type doped electron-collecting poly-Si on oxide (POLO) junction with an Al-alloyed *p*⁺ junction for hole collection. This combination can be integrated either in front- and back-contacted back junction cells (POLO-BJ) or in interdigitated back-contacted cells (POLO-IBC). Here, we present recent progress with these two cell concepts. We report on a certified M2-sized 22.9% efficient POLO-BJ cell with a temperature coefficient TC_{η} of only $-(0.3 \pm 0.02) \%_{\text{rel}}/\text{K}$ and a certified 23.7% (4 cm^2 d.a.) efficient POLO-IBC cell. We discuss various specific conceptual aspects of this technology and present a simulation-based sensitivity analysis for quantities related to the quality of the hole-collecting alloyed Al-*p*⁺ junction which are subject to continuous improvement and thus hard to predict exactly. We report that the measured pseudo fill factor values decrease more due to metallization than would be expected from recombination in the metallized regions with an ideality factor of one only. The gap to pseudo fill factor values that are theoretically achievable at the respective open-circuit voltages is 1.1%_{abs} (Ga-doped wafer) for POLO-IBC and 1.4%_{abs} (B-doped wafer) to 2%_{abs} (Ga-doped wafer) for POLO-BJ. With an embedded blocking layer for Ag crystallites in the poly-Si, we present a concept to reduce this gap.

KEYWORDS

efficiency potential, passivating contacts, POLO, poly-Si, solar cell development, temperature coefficient

1 | INTRODUCTION

Polycrystalline-Si on oxide-based passivating contacts have been introduced in the bipolar junction transistor community in the

1970s^{1–3} and already adapted into crystalline Si solar cells in the 1980s.^{4–9} Possibly due to, at that time, moderate energy conversion efficiencies limited by other aspects than the contacts and due to other challenges in the industrialization of Si solar cells, the topic got

This is an open access article under the terms of the [Creative Commons Attribution-NonCommercial-NoDerivs](https://creativecommons.org/licenses/by-nc-nd/4.0/) License, which permits use and distribution in any medium, provided the original work is properly cited, the use is non-commercial and no modifications or adaptations are made.

© 2022 The Authors. Progress in Photovoltaics: Research and Applications published by John Wiley & Sons Ltd.

out of focus at least for in public PV research for a long time. When “publically rediscovered” in 2013,^{10,11} a scientific debate started on the working principle of this junction scheme.

ISFH's junctions, initially mostly comprising a rather thick (~ 2 nm) thermally grown interfacial oxide,^{12,13} were considered as “special case” since quantum mechanical tunneling of charge carriers across the oxide—otherwise considered as the dominating transport mechanism—is unlikely for these oxide thickness values. With the pinhole model,^{14,15} an alternative transport mechanism was proposed,* and the term “poly-Si on oxide” (POLO) was coined in distinction to “tunneling oxide passivated contact” (TOPCon). Post priori, the existence of pinholes in well-passivating junctions was verified with various experimental methods such as TEM,^{16,17} selective etching,^{18,19} EBIC,^{17,20} temperature-dependent contact resistance measurements,^{21–23} and I - V measurements on small areas.²⁴ Meanwhile, it was shown theoretically that both—tunneling and pinhole-dominated junctions—allow for a high junction selectivity at least for electron-collecting junctions.²⁵ Moreover, it has recently been shown for various thermally and wet-chemically grown interfacial oxides²³ that the transition from the tunneling to pinhole-dominated transport regime upon high-temperature annealing coincides with the optimum of the passivation quality. We, therefore, consider the question “pinholes or tunneling” to be answered with “both coexisting” for most of the relevant interfacial oxide types. Since ~ 3 years, we are using wet-chemically grown interfacial oxides in our industrial relevant cell structures. We nevertheless continue to use the term “POLO” since the name “poly-Si on oxide” is independent of the transport mechanism and describes the junction scheme more accurately than “TOPCon.”† However, we acknowledge that the latter has become a kind of “brand name” and is more established in the community, just as other inaccurate terms before.²⁶

Besides basic work related to the abovementioned scientific question on the current transport mechanisms, enormous progress was achieved in the last years regarding the implementation of passivating contacts in lab-type and industrial Si solar cells. On lab-type solar cells, an efficiency of 26.1% was achieved in 2018 on a p -type POLO²-IBC structure,²⁷ while 26.0% was reached on a front- and back-contacted lab-type cell from p -type Si in 2020.²⁸ For industrialization, most groups focus on implementing an electron-collecting passivating poly-Si/SiO_x junction on the rear side of a front and back-contacted n -type cell with a “conventionally boron diffused” front junction. While this structure—which is also denoted by the term “TOPCon”—was introduced on lab scale,¹¹ research institutes like ECN,²⁹ GIT,³⁰ SERIS,³¹ and others first transferred it to industrially more relevant cell structures. In the meantime, companies have gained a lot of know-how. Full-area record efficiencies measured according to ISO 17025/IEC 6094 are approaching³² or even exceeding³³ 25%, and an efficiency of 25.4% has been announced recently.³⁴ Thus, the industrial R&D record is now less than 0.4%_{abs} below the respective record of 25.8% on small lab-type TOPCon cells.³⁵ Several companies have recently announced this n -type cell concept to be their successor of the PERC technology for mass production.^{36,37} Research institutes still contribute to the progress with

an in-depth understanding and optimization of specific building blocks such as the firing stability of the passivating contacts^{38–42} and their damage-free metallization.^{43,44}

With such a strong focus on the TOPCon cell structure given, we believe it is important to evaluate alternative industrial cell structures with passivating contacts as well.⁴⁵ “Established” players like SunPower⁴⁶ or LG⁴⁷ are focusing on IBC structures. The “ultimate cell design” might differ from that of an n -type TOPCon cell.²⁸ Based on fundamental considerations of combined contact selectivities for electron- and hole-selective contacts,^{48,49} ISFH developed its distinct cell development roadmap.⁵⁰ The first step exploits the high combined selectivity of a large-area electron-collecting n -type POLO (n POLO) and a small-area hole-collecting alloyed Al- p^+ -type (Al- p^+) contact. The latter is standard in the PERC and PERC+ technology^{51,52} and can be inexpensively formed during the metallization process without the necessity for boron diffusion or Ag metallization on this polarity. This Al- p^+ / n POLO combination can be implemented either in a front- and back-contacted structure (“POLO-BJ”)^{48,53,54} or in an IBC structure (“POLO-IBC”)^{55–57} (see Figure 1). For both cell structures, the efficiency potential—as previously simulated with state-of-the-art experimental input parameters for industrial components (screen-printed fingers, Cz material, etc.)—seems on par with other benchmarks: 24.7% for POLO-BJ and 25.5% for POLO-IBC.⁵⁰ One should note that the POLO-BJ structure⁴⁸ can be considered as an industrial version of the 26% lab-type cell.^{28,58} Recently, we have reported on both our first experimental POLO-BJ⁵⁹ and POLO-IBC cells.⁶⁰

In this special issue publication, we want to give an overview—based on the findings of 2 years of experimental work—about advantages but also about conceptual and technical challenges for ISFH's specific approach for the implementation of passivating contacts. To this end, we first report on the progress in the experimental development of POLO-BJ and POLO-IBC cells, resulting in efficiencies up to 22.9% (23.7%) for POLO-BJ (POLO-IBC, d.a. 4 cm²) so far. Next, we analyze specific aspects that have prevented us so far from exploiting the full previously simulated⁵⁰ efficiency potential and that are specific to our cell concepts.

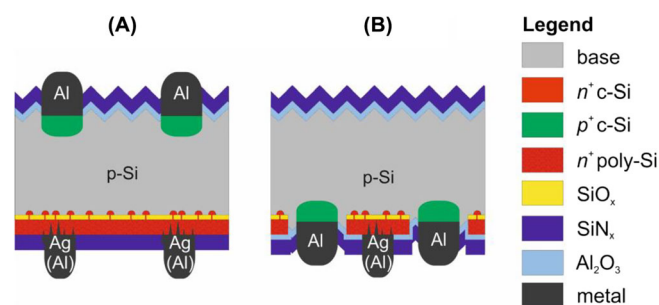


FIGURE 1 Schematic drawing of (A) the POLO back-junction (BJ) cell and (B) the POLO interdigitated back-contact (IBC) cell

For this purpose, we first perform a simulation-based sensitivity analysis to assess the impact of a variation of parameters that are “difficult to predict exactly.” This refers in particular to the quality (prefactor of recombination current density J_{0Alp^+} , specific contact resistance ρ_c) of the Al- p^+ regions. In Kruse et al.,⁵⁰ we assumed $J_{0Alp^+} = 400 \text{ fA/cm}^2$, $\rho_c = 1.3 \text{ m}\Omega\text{cm}^2$ as measured on reference samples processed alongside with PERC+ cells.⁶¹ However, the presence of n POLO junctions in our POLO-BJ and POLO-IBC cells implies some constraints, in particular regarding the maximum applicable firing temperature. To not harm the passivation quality of the n POLO junctions in the metallized regions, the firing temperature has to be significantly lower than for PERC(+) cells. Furthermore, the specific geometry of our Al fingers on the front side of the POLO-BJ cells impacts the formation of the Al- p^+ regions. These reasons result in a less perfect formation of the Al- p^+ regions in our POLO-BJ⁵³ and POLO-IBC cells⁵⁷ so far and consequently in higher J_{0Alp^+} values than assumed in the simulation paper by Kruse et al.⁵⁰

Second, we analyze in detail the pseudo fill factor of our devices on precursor and full cell level. By comparison with theoretical expectations, we reveal that the recombination behavior in our cells is compromised upon metallization by additional issues besides an increase of surface recombination paths with an ideality factor of one. While we review different hypotheses for the root cause of this issue, it is clear that the n POLO junctions act as “emitter” in our cells. Therefore, spiking of Ag crystallites through the poly-Si can cause recombination in the space charge region with an increased ideality factor, as well as shunts. Since, nevertheless, sufficiently high firing temperatures are necessary, particularly for improving the Al-alloyed p^+ -based hole-collecting junctions, we present a novel concept of an embedded blocking layer for Ag crystallites in the poly-Si.

A potential advantage of our approach—thanks to the higher open-circuit voltage compared to PERC—is expected in the temperature behavior. We, therefore, investigate this aspect by following a recent directing work of Le et al.⁶² We measure a temperature coefficient of only $-(0.3 \pm 0.02) \text{ \%}_{\text{rel}}/\text{K}$ for the efficiency of our POLO-BJ cell.

2 | RECENT IMPROVEMENT OF ENERGY CONVERSION EFFICIENCY AND INTERPRETATION OF DEVICE PHYSICS

In Table 1, we have listed our latest I - V results for our so far best POLO-BJ and POLO-IBC cells, as independently confirmed by ISFH CalTeC, compared to other high-temperature process-based record cells.

The 22.9% efficient POLO-BJ cell is described in detail in Min et al.⁵⁹ Briefly summarized, the improvement as compared to the 22.6% reported in a previous publication⁵⁴ is achieved by an improved shape of the front-side Al fingers (finger width only $60 \mu\text{m}$, high aspect ratio) and by increasing the Al- p^+ thickness. The latter results in a reduction of the pre-factor of the recombination current density J_{0Alp^+} from a previous value of 2800 fA/cm^2 ⁵³ down to 830 fA/cm^2 (as concluded from a comparison of the measured I - V curves with numerical device simulations based on Quokka2⁶³).

For our improvement of the efficiency of the POLO-IBC cell from 23% as described in Haase et al.⁵⁷ to 23.7% (4 cm^2 d.a.), we implemented a smaller Al- p^+ contact width, which reduces not only the area-weighted recombination but also J_{0Alp^+} itself by increasing the Al- p^+ thickness. We quantified J_{0Alp^+} for our POLO-IBC cells by comparing experimental results and numerical device simulations using PC3D.⁶⁴ Processing many small-area cells with different geometries (different Al- p^+ area fractions, but also different pitches, emitter coverage fractions, etc.) provides an comprehensive set of data that strongly narrows down the possible simulation input parameters providing a consistent agreement. The resulting saturation current density value J_{0Alp^+} for POLO-IBC is 600 fA/cm^2 —which is a clear improvement as compared to the previous J_{0Alp^+} value of 2250 fA/cm^2 .⁵⁷ For POLO-IBC, we furthermore increased the photo-generation by a double antireflection coating (DARC). The latter is of course not relevant on module level but quite common on record cell level—even for industrial-like solar cells.

While our current experimental results represent an interim status after ~ 2 years of development, we think that they are promising.

TABLE 1 Comparison of the main IV parameters obtained on our so far best experimental POLO-IBC and POLO-BJ cells with the predictions from simulations (input values from Table 2, values of brackets, if a range is mentioned) and with recent records for the industrial high-temperature benchmarks TOPCon and PERC

Cell structure	η (%)	V_{oc} (mV)	FF (%)	J_{sc} (mA/cm^2)	Area (cm^2)	Ref.
POLO-IBC (simulated potential)	25.3	736	83.2	41.3 (no DARC)	Unit cell	This work
POLO-IBC (measured)	23.71	711.5	80.9	41.3 (DARC)	4 (d.a.)	This work
POLO-BJ (simulated potential)	24.5	733	82.9	40.3	Unit cell	This work
POLO-BJ (measured)	22.9	714	80.9	39.6	244 (full area BB-less)	59
TOPCon/Longi (measured)	25.2	722	83.9	41.6	243 (aperture area)	35
TOPCon/Jinko (measured*)	25.4	-	-	-	264	34
TOPCon/Trina (measured)	24.6	717	84.5	40.6	244 (full area)	32
TOPCon/Jolywood (measured)	24	703	84.5	40.4	252	65
PERC/Longi (measured)	24	694	83.3	41.6	244.6 (full area)	35

Note: Measured IV data are independently confirmed and, except (*), ISO 17025/IEC 6094 calibrated.

In particular, the open-circuit voltages up to 714 mV are on par with that reported for record TOPCon cells^{32,35,65} and significantly higher than the 694 mV reported for the best PERC cell.³⁵ Since the latter also has Al-alloyed p^+ hole-selective contacts, this comparison clearly proves that the passivating electron-collecting n POLO junction facilitates higher V_{oc} values than a conventionally phosphorus-diffused emitter.

The comparison in Table 1 also shows that we are not exploiting our technology's full simulated efficiency potential yet. This requires further analysis—as provided in Sections 3 and 4. Here, we would like to first introduce our picture of the interpretation of the device physics as used in the following. Our picture is strongly influenced by the two-diode model that is well established in the PV community. Within this framework, the total recombination current density of the cell with a voltage-dependent ideality factor is resulting from a superposition of different recombination paths with voltage-independent ideality factors. The voltage dependence of different important recombination paths such as radiative recombination in the entire injection-level range, Auger recombination in low-level injection and Shockley–Read–Hall recombination in low-level injection can be described with an ideality factor of 1. In the two-diode model, they are lumped into a diode with a saturation current density J_{01} , which is the sum of the respective values of all these paths. In numerical device simulators based on the conductive boundary model⁶⁶ such as Quokka or PC3D, the voltage dependence of the recombination at most of the surfaces is described by an ideality factor of 1. This is justified when considering the inherent (unperturbed) recombination properties of doped surfaces, of undoped surfaces passivated by charged dielectrics,⁶⁷ and for most passivating contact schemes. However, the voltage-dependent ideality factor of the total recombination is often larger than 1 in real devices. This can (partially) taken into account in the two-diode model with a second diode, exhibiting an ideality factor of 2. Typically, the presence of this additional diode is associated with Shockley–Read–Hall recombination in regions where the hole and electron concentrations are of similar order of magnitude. This could be the case in the space charge region of the pn junction but also in the wafer bulk if the device is in high-level injection. Shockley–Read–Hall recombination at undoped surfaces might also occur under high-level injection either if a surface passivation scheme with a rather low density of fixed charges (e.g., SiO_x) is applied or if scratches, blisters, or other process-induced degradation mechanisms (locally) compromise the surface passivation quality.⁶⁸ Within the framework of the two-diode model, an increased ideality factor of the total I - V curve can also be implied by a finite shunt resistance at lower voltages and by the series resistance at higher voltages. Although the (dark and light) I - V and J_{sc} - V_{oc} curves of our cells can be well described by the two-diode model, we do not want to limit ourselves to this simplified view. It is well known that also further effects such as transport-limited recombination, edge effects, inhomogeneities, and resulting balancing currents⁶⁹ can contribute to an increased ideality factor. It is also possible (and even desirable) that Auger bulk recombination in high-level injection with an ideality

factor of 2/3 is one of the major remaining paths, facilitating an ideality factor of the total recombination smaller than 1.

When describing surface recombination processes in the following, we distinguish between recombination paths that are related to an ideality factor of one (and increase the corresponding saturation current density J_{01}) or that contribute to an increased ideality factor.

3 | SENSITIVITY ANALYSIS FOR HARD-TO-PREDICT INPUT PARAMETERS

While we made—mainly thanks to excellent cooperation with Toyo Aluminium—good progress in improving the quality of the Al- p^+ regions under our specific constraints and although further improvement is ongoing, the development of the parameters J_{0Alp^+} and ρ_c is hard to predict precisely. We therefore perform a sensitivity analysis of the device performance with respect to these parameters. Since the optimal area fraction for the Al- p^+ regions results from balancing recombination losses with lateral transport losses for a given J_{0Alp^+} and ρ_c value pair, we also include the wafer doping level and the area fraction of the Al- p^+ regions in our analysis.

One should note that while the difference of the quality of our actual Al- p^+ regions and the respective assumptions in Kruse et al⁵⁰ is one important reason for the discrepancy between the simulated efficiency potential and the current experimental status, there are also other aspects compromising so far the efficiency in our experimental devices. However, although they are possibly of comparable importance, most of them can hardly be described within the framework of a unit cell simulation. Therefore, we discuss many of these aspects qualitatively in the analysis of our pseudo fill factor pFF values below.

For the sensitivity analysis, we use Quokka2⁶³ for the simulation of the POLO-BJ and PC3D⁶⁴ for the simulation of the POLO-IBC structure. Since the analysis yields qualitatively comparable results for POLO-BJ and POLO-IBC, we restrict ourselves to one structure (POLO-IBC) in the following.

The predictable-with-high-confidence parameters are fixed, whereas the hard-to-predict-exactly parameters are varied as described above. Table 2 lists all of our input parameters, fixed values, and range of parameters. The values in brackets are the measured values on the current devices or test samples. One should note that although it is possible to also include imperfections such as parallel current paths via shunts or surface recombination losses with an ideality factor of 2 in these models, we restrict ourselves at this point to the assumption of surface recombination with an ideality factor of 1 only and a high external R_{shunt} . As we will show below, this (optimistic) approach cannot describe all losses in our current devices. Nevertheless, it can reveal the impact of the quality of the Al- p^+ regions on the performance of our devices.

We perform 25 simulations with different combinations of input parameters with the rules of design of experiment analysis.

Figure 2 shows the predicted results of our POLO-IBC simulations. The figure shows five-by-four graphs. On the y-axis, we show the different cell parameters as a function of one of our varied input

TABLE 2 Input parameters for the unit cell simulation of POLO-IBC. The values in brackets refer to the current experimental values

Parameter	Value
Wafer thickness (μm)	160
Minority carrier bulk lifetime τ_{n0} (μs)	2000
Majority carrier bulk lifetime τ_{p0} (μs)	20,000
Wafer resistivity ρ_b ($\Omega\text{ cm}$)	0.6–1.2 (0.9)
Al- p^+ contact fraction (%)	0.4–1.5 (0.76)
Al finger width (μm)	100
Ag finger pitch (μm)	988
nPOLO emitter rear coverage (%)	73
nPOLO emitter contact width (μm)	60
J_{0e} nPOLO emitter with and without contact (fA/cm^2)	2
$J_{0-\text{Al-}p^+}$ base contact (fA/cm^2)	100–1000 (600)
$J_{0-\text{AlOx}/\text{SiNy}}$ passivation front side and base finger (fA/cm^2)	2
R_{sheet} nPOLO emitter (Ω)	80
ρ_c Ag/nPOLO emitter contact ($\text{m}\Omega\text{ cm}^2$)	0.9
ρ_c Al- p^+ base contact ($\text{m}\Omega\text{ cm}^2$)	0.1–1.3 (0.8)
R_{shunt} ($\Omega\text{ cm}^2$)	10,000

parameters. On the x -axis, we show the four different varied input parameters. In every graph, the dashed line marks the value for the parameter, which is used in the other three variations on the x -axis. It is also listed in Table 2 in brackets.

With decreasing Al- p^+ contact resistivity ρ_c from 1.3 to 0.1 $\Omega\text{ cm}^2$, the short-circuit current density J_{sc} and the open-circuit voltage V_{oc} do not change. Still, the FF increases from 82.8% to 83.8% since the series resistance decreases. Hence, the efficiency also increases from 25.1% to 25.5%.

With decreasing Al- p^+ contact recombination factor $J_{0\text{Al}p^+}$ from 1000 to 100 fA/cm^2 , V_{oc} is increased by 1.5% relative. This also results in an increased pseudo fill factor. Since a reduction of recombination at high-low junctions is also relevant under short-circuit conditions (due to the remaining split of the quasi-Fermi levels at this location), the J_{sc} is increased as well. Overall, the efficiency increases to 25.5%.

With increasing Al- p^+ area fraction from 0.4% to 1.5%, the FF increases the most by 4.1%_{rel} mainly due to reduced series resistance at the contact and in the bulk. V_{oc} , J_{sc} , and pFF decrease by 0.9%_{rel}, 2.0%_{rel}, and 0.5%_{rel} due to increased recombination at the contacts. Hence, the efficiency shows a maximum of 25.3% for 1.0% Al- p^+ area fraction.

With decreasing bulk resistivity ρ_b from 1.2 Ω to 0.6 $\Omega\text{ cm}$, the FF increases the most by 1.0%_{rel} due to less series resistance in the bulk. The pFF , V_{oc} , and J_{sc} decrease by 0.5%_{rel}, 0.1%_{rel}, and 0.9%_{rel} due to increased recombination. Hence, the efficiency is 25.3%, nearly independent of the bulk resistivity in the simulated range. This is a positive finding since it allows for using a wide resistivity range present in an ingot.

To summarize, the sensitivity analysis shows that the reduction of Al- p^+ recombination and resistance is of high importance—for POLO-IBC, but in a similar manner also for POLO-BJ (not shown). By contrast, our current experimental values for the base doping and the Al- p^+ area fraction are already close to the respective optimum values. It is not possible to further compensate a low Al- p^+ quality—in terms of both high $J_{0\text{Al}p^+}$ and ρ_c —by adjusting the base doping and the Al- p^+ area fraction. This is also expected from our fundamental considerations of the selectivity of otherwise ideal solar cells: In Schmidt et al.,⁴⁹ figure 10 shows that the optimal area fraction of a contact with our current parameters— $J_{0\text{Al}p^+} = 600\text{ fA}/\text{cm}^2$, $\rho_c = 0.8\text{ m}\Omega\text{ cm}^2$ —is $\sim 0.3\%$. Since these calculations are based on the simple one-diode model and thus do not include further extrinsic losses like transport losses for holes in the wafer, our more realistic device simulations yield slightly higher values for the optimal area Al- p^+ fraction: 0.9% for POLO-BJ and 0.7% for POLO-IBC.

Most important, we obtain consistent results to the previous work of Kruse et al.⁵⁰ when assuming comparable low $J_{0\text{Al}p^+}$ values of 400 fA/cm^2 (our experimental ρ_c value of 0.8 $\text{m}\Omega\text{ cm}^2$ is already lower than the 1.3 $\text{m}\Omega\text{ cm}^2$ assumed by Kruse et al.⁵⁰). A $J_{0\text{Al}p^+}$ value of 400 fA/cm^2 or below is compatible with a high efficiency potential of 24.6% for POLO-BJ and 25.4% for POLO-IBC.

4 | (PSEUDO) FILL FACTOR ANALYSIS

As mentioned above, the unit cell simulations performed for our sensitivity analysis do not include all loss channels present in our experimental cells. Therefore, they overestimate the efficiency for the reference point of the current $J_{0\text{Al}p^+}$ and ρ_c values. This is in particular obvious in the fill factor values. Remarkably, also as compared to the fill factor values of the TOPCon cells (Table 1), our experimental FF values fall short. One might also take the perspective that the fill factor values up to 84.5%^{32,65} reported for the TOPCon cells are remarkably high. Nevertheless, an even higher FF value of 86.6% has been reported recently on a large-area hydrogen-rich amorphous Si/c-Si heterojunction cell with nine busbars by Longi.⁷⁰ Such high fill factors have two prerequisites: high pseudo fill factors $> 85\%$ as implied by a “favorable” recombination behavior and low series resistance values.

As shown in Figure 2, the unit cell simulations predict high pseudo fill factors of $\sim 85.5\%$ on our POLO-IBC cells for our current quality of the Al- p^+ regions. The actual measured values of 83.9% (see below) are significantly lower. However, the unit cell simulations also predict the open-circuit voltage to be $\sim 25\text{ mV}$ larger than our measured values.

At this point, it is not clear whether our lower pFF values are a consequence of the lower V_{oc} (i.e., a consequence of higher-than-expected surface recombination with an ideality factor of 1) or whether additional issues compromise the pseudo fill factor in our devices. In the following subsection, we, therefore, analyze the pseudo fill factor \ddagger for our technology in order to deduce a strategy for how to increase the fill factor.

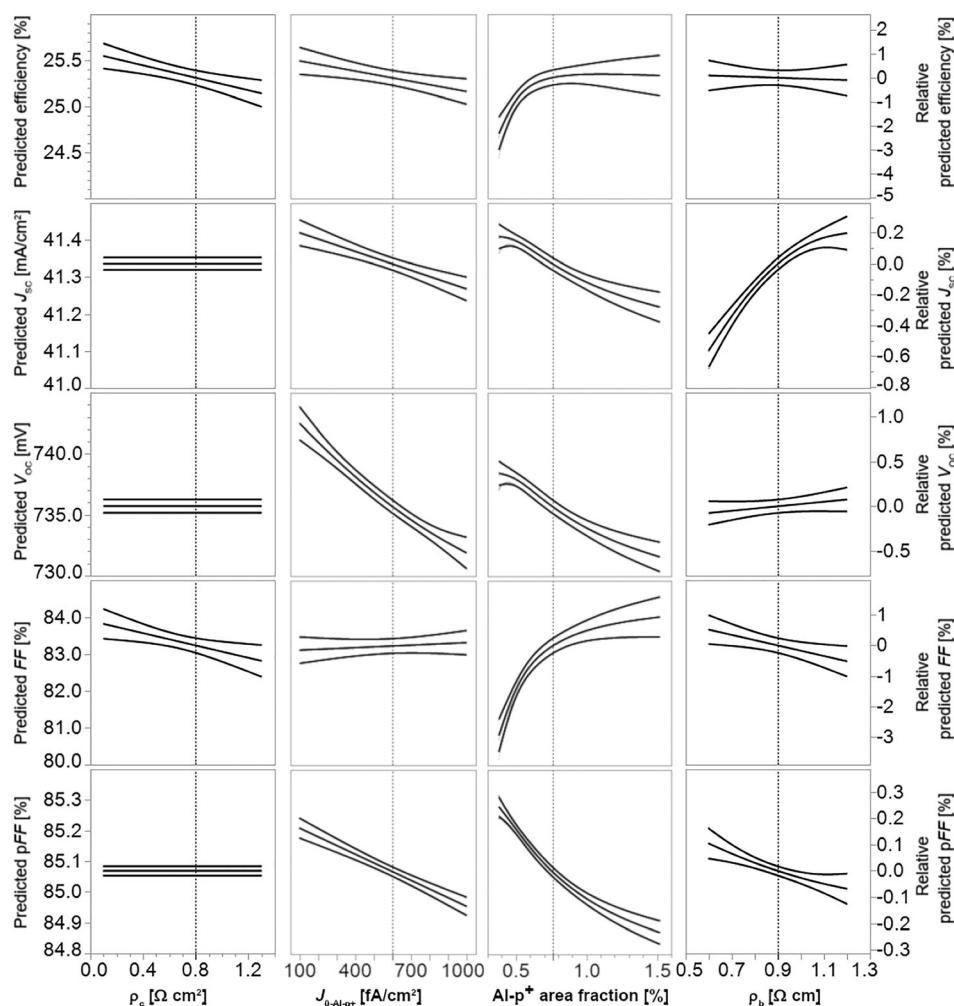


FIGURE 2 Predicted response graph of the design of experiments simulation study for the POLO-IBC cell. Each graph shows the predicted result with an upper and lower confidence interval. The y-axis shows the predicted IV parameters in absolute values on the left and relative values on the right in dependence of the four varied input parameters on the x-axis. In every graph, the dashed line marks the value for the parameter, which is used in the other three variations on the x-axis. Upper and lower curves indicate the interval of confidence

For this purpose, we calculate which pseudo fill factor values can be expected for the V_{oc} values actually measured on our cells—first assuming that the surfaces only imply recombination with an ideality factor of 1. These calculations are based on one-dimensional Quokka2 simulations with a highly idealized cell structure: The front side is assumed to be perfectly passivated. The rear-side passivation is swept from perfect passivation ($J_{0, rear} = 0.01 \text{ fA/cm}^2$) to a metallized scenario ($J_{0, rear} = 1000 \text{ fA/cm}^2$). This—in combination with the recombination in the bulk—determines the V_{oc} of the device. The wafer thickness is set to $160 \mu\text{m}$, and the base doping is $1 \Omega\text{cm}$ in all cases. The parameterization from Richter et al.⁷¹—as implemented in Quokka2—is used for the intrinsic (Auger, radiative) bulk recombination. For the Shockley–Read–Hall recombination in the bulk, we considered three scenarios: (i) no SRH recombination, that is, “infinite” high τ_{SRH} values to access the intrinsic limit, (ii) a state-of-the-art deactivation of BO complexes according to the parameterization of Walter et al.⁷² (valid for $[O_i] \sim 5 \cdot 10^{17} \dots 10^{18} \text{ cm}^{-3}$), and (iii) an injection-independent bulk lifetime $\tau_{SRH, fix}$ which represents Ga-doped p-type material. For the latter case, we swept $\tau_{SRH, fix}$ from $100 \mu\text{s}$ to 0.1 s . We also applied the “ $\tau_{SRH, fix}$ ” scenario to n-type material with $1\text{-}\Omega\text{cm}$ base resistivity.

Generation current density is set to 42 mA/cm^2 . Since no further series resistance contributions are taken into account, the simulated fill factor should be determined by the recombination behavior only and thus be comparable to the pseudo fill factor of our cells.

Figure 3 compares the simulated pseudo fill factors with the experimentally measured values. Let us discuss the simulation results first: Regarding the “intrinsic bulk recombination limit” for p type (black line), it is obvious that the pseudo fill factor is increasing with increasing surface passivation quality. In particular, if the latter enables V_{oc} values of $\sim 725 \text{ mV}$ or larger, the pFF steeply increases well above 85%. For a V_{oc} value of 750 mV —as achieved by Longi on their record Si heterojunction cell⁷⁰—the pFF reaches 87.7%. This is because the injection level is approaching the same order of magnitude as the doping concentration, resulting in a decrease of the ideality factor of the Auger recombination in the bulk from 1 to 2/3. The “intrinsic bulk recombination” limit pFF (V_{oc}) curve is also approached for the “injection-independent” bulk lifetime scenario (cyan symbols) representing Ga-doped materials for sufficiently high $\tau_{SRH, fix}$ values. For a $J_{0, rear}$ value of 10 fA/cm^2 , for example, a $\tau_{SRH, fix}$ value of 1, 10, and 100 ms enables a pFF value of 84.62%, 85.65%, and 85.86%, respectively. Obviously, pFF ($\tau_{SRH, fix}$) saturates when $\tau_{SRH, fix}$ is

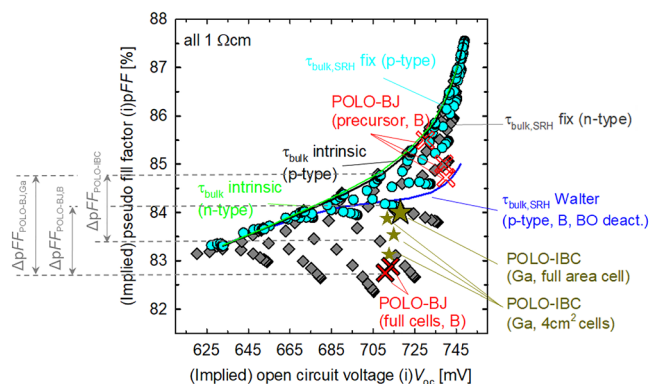


FIGURE 3 Simulated pseudo fill factor values for specific assumptions on the bulk lifetime (lines, cyan, and gray symbols) as a function of the open-circuit voltage V_{OC} . The latter is exclusively varied by sweeping the prefactor of a recombination with an ideality factor of one at the rear side of an otherwise ideal cell from 0.01 to 1000 fA/cm² (lines = specific $\tau_{bulk,SRH}$ parameterizations) or by furthermore sweeping injection-level independent $\tau_{bulk,SRH}$ values from 100 μ s to 0.1 s (cyan and gray circles). Also shown are our experimental values, either extracted from the implied I - V curve on cell precursor level (open red crosses for POLO-BJ) or from J_{sc} - V_{OC} curves on full cells (POLO-BJ: filled red crosses, POLO-IBC: filled stars). All values refer to a base resistivity of ~ 1 Ω cm and a wafer thickness of 160 μ m

approaching 10 ms since the dominating recombination mechanism is shifting from SRH to intrinsic recombination in this regime. This again verifies previous knowledge that excellent p -type material with high injection-level-independent SRH lifetimes $\tau_{SRH,fix}$ —such as FZ or Ga-doped Cz—enables as high pseudo fill factor values as n -type material.^{27,28}

It is interesting to note that a certain V_{OC} value can be reached by different combinations of $J_{O,rear}$ and $\tau_{SRH,fix}$, which do not yield the same pFF values. This is the reason for the apparent branches in Figure 3. Interestingly, the lowest pFF values for a given V_{OC} correspond to intermediate $\tau_{SRH,fix}$ values which are sufficiently high to enable high injection-level conditions but still sufficiently low to cause significant SRH recombination—in this case with an ideality factor between 1 and 2. This effect is even more pronounced for the n -type material (gray diamonds) since the chosen base resistivity of 1 Ω cm corresponds to a lower doping concentration ($N_D = 5 \cdot 10^{15}$ cm⁻³) than for the p -type material ($N_A = 1.5 \cdot 10^{16}$ cm⁻³). Thus, the high-level injection conditions play a larger role. This points to the fact that an improvement of surface passivation has to go hand in hand with an improvement of the bulk material in order to achieve both—highest V_{OC} and pFF values.

When now comparing the abovementioned model predictions for material with injection-level-independent SRH lifetimes (e.g., Ga-doped p -type Cz) with the predictions for boron-doped material with the best BO complex deactivation reported so far⁷² (see blue curve in Figure 3), a significant difference in the pFF values is observed for higher V_{OC} values. The remaining (weak) injection-level dependency of

τ_{SRH} for the boron-doped material is predicted to prevent pFF values above 85% even for the best surface passivation quality. This might be considered a fundamental disadvantage of boron-doped Cz material, even if the deactivation of the BO complexes is permanent. However, the parameterization of Walter et al⁷² is based on experimental values and, therefore, not carved in stone. Higher lifetimes and less pronounced injection-level dependencies could be facilitated, for example, by lower $[O_i]$ concentrations than considered by Walter et al (i.e., $< 5 \cdot 10^{17}$ cm⁻³). Indeed, we have already measured lifetimes on Al₂O₃-passivated boron-doped Cz material⁵⁰ which exceeds the parameterization of Walter et al⁷² and also enabled higher iV_{OC} , ipFF pairs (745 mV, 86.2%)⁵⁰ than predicted according to Figure 3.

In the following, we compare our experimental (implied) pFF values to these predictions. We first measure the implied I - V characteristic by the photoconductance decay method on cell precursors without metallization (front-side textured and Al₂O₃/SiN_x passivated, rear-side planar with n POLO junctions capped with Al₂O₃/SiN_x, fired, BO deactivation). QSSPC measurements are only reliable on the POLO-BJ structure since the structured rear side of the POLO-IBC cell would affect the eddy currents. Since QSSPC is a spot measurement, we cannot exclude—although we averaged across five positions on the wafer—that the recombination behavior is different (worse) in some regions, for example, the wafer edge. All POLO-BJ precursors that we have fabricated so far use boron-doped material. The open red crosses in Figure 3 show promising (iV_{OC} , ipFF)—pairs with highest iV_{OC} values up to 740 mV and highest ipFF values up to 85.5%. All these data points show higher ipFF values than predicted by the simulation based on the BO parameterization by Walter et al (compare blue curve in Figure 3). The highest ipFF value of 85.5% even approaches the “intrinsic bulk recombination limit” for the corresponding iV_{OC} value of 730 mV. This is another example of an exceedance of the parameterization of Walter et al.⁷² These findings show not only the high quality of our surface passivation schemes including the fired n POLO junction on the rear but also verify a high SRH bulk lifetime τ_{SRH} in our samples. Obviously, there is also no or only a minor contamination issue at this stage. The (i)pFF values of these p -type cell precursors are on par with those achievable on n -type material. Recombination in the bulk does not limit our fill factor values.

When applying the metallization, the surface recombination is increased (as compared to the precursor level) due to the—in this stage present for the first time—Al- p^+ hole-collecting contacts. While we cannot fully exclude a deterioration of the passivation quality of the n POLO junction in the Ag metallized regions as well, numerous analyses (not shown) indicate that this is—if present at all—a small effect in terms of additional recombination with an ideality factor of 1. The resulting open-circuit voltages from 711 to 718 mV measured on our best devices so far are lower than expected from device simulations (compare, e.g., 736 mV (733 mV) for POLO-BJ (POLO-IBC) according to Kruse et al⁵⁰). However, the essential point here is that the pFF values measured on these cells are much lower than predicted by the simulations and lower than expected from the promising results on precursor level. For the POLO-BJ cell (filled red crosses in

Figure 3), the best measured pFF of 82.9% is $\sim 2\%_{\text{abs}}$ smaller than the “intrinsic bulk recombination limit” and $\sim 1.4\%_{\text{abs}}$ smaller the predictions of the BO deactivation according to Walter et al⁷² at the measured V_{oc} value of 713 mV. One might speculate that the BO defect deactivation process is affecting the full cells differently (i.e., less efficient) than the cell precursors⁷³ but also the POLO-IBC cells—made of Ga-doped *p*-type Cz material—show low pFF values (compare golden stars in Figure 3). Since some of our POLO-IBC cells are measured on 4 cm² designated area (small golden stars), one hypothesis for the low pFF values $\leq 83.9\%$, in this case, could be perimeter losses. However, we have quantified these parameter losses on lab-type IBC cells with the same dimensions and base doping density to be only $\sim 0.25\%_{\text{abs}}$.⁷⁴ Here, we are missing at least $1\%_{\text{abs}}$ to the “intrinsic bulk recombination limit.” Furthermore, we also measured $J_{\text{sc}}-V_{\text{oc}}$ curves on full-area illuminated M2-sized POLO-IBC cells (large golden star in Figure 3). Here, the pFF is only $0.1\%_{\text{abs}}$ larger than of the best small-area cell and still $1.1\%_{\text{abs}}$ below the “intrinsic bulk recombination limit.”

Obviously, the recombination behavior in our full cells is compromised in a manner that the pFF—and thus the final fill factor—is reduced by $1\%_{\text{abs}}-2\%_{\text{abs}}$ compared to the limit implied by the bulk material and surface recombination with an ideality factor of 1. There are different possible reasons: (i) balancing currents between different recombination-active areas in the cell, (ii) shunting issues implied by the (emitter) metallization, (iii) additional contaminations implied by the metallization process, and (iv) surface recombination in the metallized regions with an ideality factor larger than 1.

Regarding hypothesis (i), one supporting argument is that if there is an inhomogeneity in the passivation quality of the *n*POLO junctions, it will result in stronger pronounced balancing currents for electrons and holes (the latter through the wafer) than in the case of an *n*-type substrate. One counterargument is that the pFF is also reduced on the small-area POLO-IBC cells. Passivation quality is quite homogeneous across this small area. It is also rather homogeneous across the entire wafer, as shown by lifetime maps and photoluminescence and electroluminescence measurements on final cells. Regarding hypothesis (ii), we analyze the parallel resistance R_{shunt} as determined from the reverse $I-V$ curve (-0.5 V) based on the two-diode model. In our firing temperature variations, we find many cells with $R_{\text{shunt}} < 10$ k Ωcm^2 for nonoptimal firing conditions (too high firing temperatures). Obviously, the firing process window is quite narrow since the *n*POLO junction poses the emitter in our cells, and any penetration of Ag crystallites through the poly-Si may short-circuit the cell. This is a disadvantage compared to a TOPCon cell where the *n*-type poly-Si/SiO_x is the base contact.

Nevertheless, our best cells fired at the optimum temperature all exhibit R_{shunt} values > 4 (10) k Ωcm^2 on POLO-BJ (POLO-IBC)—and still show the reduced pFF values depicted in Figure 3. Although we attempt to widen the firing process window (see Section 5), a shunting issue is not our leading hypothesis for the pFF limitation in our best cells. Hypothesis (iii) is not supported by any indication so far. From the high (iV_{oc} , $ipFF$) pairs measured on the fired precursors (see above), we conclude that the firing process itself does not introduce further contaminations. Regarding hypothesis (iv), it appears

plausible that Ag crystallites penetrating through the poly-Si could reach the space charge region of the *pn* junction, causing recombination with an increased ideality factor. Nevertheless, also the Al-based metallization could contribute to the unfavorable recombination behavior. It is known that the Al-alloyed *p*+ regions can cause recombination with an increased ideality factor, in particular, if they are not perfectly formed out.⁷⁵ Indeed, we have observed that—possibly implied by the constraints on the applicable firing temperature for a shunt-free metallization of the *n*POLO junctions—the Al-*p*+ regions in our cells exhibit increased recombination with an ideality factor of 1 than reported for PERC cells.^{53,57} For the dash contacts applied on our POLO-IBC cells, the *p*+ depth at the endings is significantly reduced.⁵⁷ Also, for the point contacts applied to the front side of the POLO-BJ cell, a further increase in the depth of the Al-*p*+ region would be desirable.⁵³ However, we have also varied the area fraction of the Al-*p*+ regions on our POLO-IBC cells—without finding a clear correlation between an increased Al-*p*+ area fraction and a reduced pFF. This indicates that the Al-*p*+ regions themselves seem not to be the origin of the increased ideality factor. However, the Al metallization might still comprise the recombination behavior by other effects such as spiking of the Al through the Al₂O₃/SiN_x passivation stack aside of the LCO regions.⁶⁰

To summarize, we do not have a consistent picture of the root cause of the reduced pFF values measured on our cells yet, and further research is required here to transfer the high measured pFF values of up to 85.5% for POLO-BJ precursors to metallized POLO-BJ and POLO-IBC devices. In this regard, improving the robustness of the *n*POLO junction against a spiking-through of Ag-crystallites—even at higher firing temperatures and even for thinner poly-Si layers—would be desirable. It would mitigate shunting issues and prevent possible recombination with increased ideality factor in the space charge region of the *pn* junction. Higher firing temperatures would facilitate the improvement of the Al-*p*+ regions in terms of reducing recombination with an ideality of 1, and, if present, with a higher ideality factor. Thinner poly-Si layers would reduce free carrier absorption.

5 | CONCEPT OF AN EMBEDDED BLOCKING LAYER

For increasing the robustness of the *n*POLO junction against a spiking-through of Ag-crystallites, tailoring the in-diffused P profile—either by an optimization of the interplay between the interfacial oxide, temperature budget for the POLO junction formation, and the doping concentration in the poly-Si^{43,65} or by an additional weak P diffusion performed prior to the poly-Si deposition—is an obvious approach. Here, we introduce an alternative new concept: We are working on a barrier layer embedded in the poly-Si, which should stop the Ag crystallites before reaching the SiO_x/c-Si interface. For this purpose, different dielectric and conductive layers are evaluated. Our front-up approach is a thin SiO_x—as used for the interface between the poly-Si and the Si. Indeed, most of the Ag crystallites penetrating through the poly-Si do stop at the c-Si/SiO_x interface according to

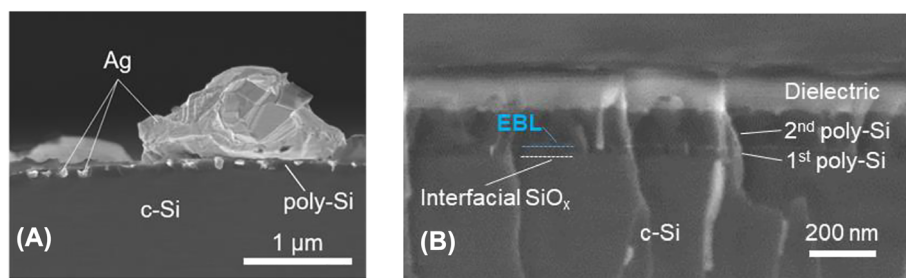


FIGURE 4 (A): Scanning electron microscope (SEM) cross-sectional image of a metallized *n*POLO junction, showing the stopping of the Ag crystallites at the c-Si/SiO_x interface. (B) SEM cross-sectional image of a (non-metallized) *n*POLO junction with embedded blocking layer (EBL). The latter consists of a thin SiO_x layer

our SEM cross-sectional measurements (Figure 4A). One speculative hypothesis is that the glass components of the paste that typically enable penetration of the paste through the dielectric layers on top of the poly-Si do not reach the buried SiO_x layer, which thus does not dissolve. Another hypothesis is that the formation of Ag crystallites depends on the crystal orientation in the (poly) Si. Also, in this case, an amorphous blocking layer can yield different orientations of the crystallites in the lower and the upper poly-Si layer, preventing grains favorable for Ag penetration vertically extending through the entire poly-Si. The embedded blocking layer needs to allow a current flow from the poly-Si on top (in contact with the Ag crystallites) and the poly-Si below. Also, for this reason, it appears plausible to start with a SiO_x layer which already has proven to facilitate efficient electron transport by either pinhole formation or tunneling.

We evaluated the passivation quality of a stack of a wet-chemically grown interfacial oxide (ozone diluted in deionized water, 1.5 nm thickness according to ellipsometry), a first in situ *n*-type doped LPCVD poly-Si layer with a thickness of 30 nm, an ex situ thermally grown embedded SiO_x blocking layer (EBL) with a thickness of 1.5 nm (measured on polished reference samples with ellipsometry), and a second in situ *n*-type doped LPCVD poly-Si layer with a final thickness of 140 nm. Figure 4B shows an SEM cross-sectional image of this stack. After junction formation at 860°C, deposition of an Al₂O₃/SiN_x hydrogen donor layer stack, and firing, we determined a J_0 value of 6 fA/cm² per side (implied open-circuit voltage at 1 sun = 725 mV) on symmetric lifetime test structures. Although we typically obtain lower J_0 values, also the reference group without embedded blocking layer performed equally in this batch. We, therefore, conclude that—as expected—the EBL does not influence the passivation quality of the POLO junctions. An evaluation of its potential benefit, that is, of its Ag blocking capability, is still ongoing on cell level. In perspective, one can imagine in situ grown EBLs for LPCVD as well as for other deposition techniques (PECVD, APCVD, etc.).

6 | TEMPERATURE COEFFICIENT

Besides the experimental demonstration of the high simulated efficiency potential, we are working on the elaboration of further positive aspects of our technology. One cost-saving potential is the

application of an “all-Al”§ metallization, that is, a non-alloying Al paste for contacting the poly-Si. We have recently reported on a proof-of-concept POLO-BJ cell with this metallization scheme.⁵⁹ A further potential advantage is—compared to PERC—a reduced temperature coefficient, which we expect from the high open-circuit voltage. A comprehensive work on this aspect for TOPCon cells has recently been published by Le et al.⁶² In the following, we report on our first evaluation of temperature coefficients of our technology, exemplarily measured on POLO-BJ cells. We compare POLO-BJ cells based on B-doped and Ga-doped wafers in order to take into account the effect of an injection-level dependency of the bulk lifetime—if present at all.

We perform these measurements on a LOANA *I*-*V* tester from pvtools. We either set the wafer temperature to the highest set point (65°C) and decrease it by 10°C from measurement to measurement (“downward measurement” in Figure 5) or start from 25°C while increasing the temperature between the measurements (“upward measurement” in Figure 5). This check for consistency is successful (see Figure 5). We report all *I*-*V* values for the temperature actually measured by the sensor below the wafer. We estimate the uncertainty in the wafer temperature to $\pm 3^\circ\text{C}$.

Figure 5 shows the main *I*-*V* parameters as a function of the temperature. Also, the results from linear regression are given in terms of relative values. The uncertainties specified for the temperature coefficients of the efficiency, the short-circuit current, and the open-circuit voltage are adapted from ISFH CalTeC, assuming that our in-house measurement system implies similar values.

Although the absolute values of the boron-doped and the Ga-doped POLO-BJ cell differ from each other, linear regression results in almost identical values. This is consistent with our finding above that the (p)FF of our cells is not limited by injection-dependent bulk recombination—even not for cells on boron-doped material. (Otherwise, we would have expected a different temperature dependence of the (p)FF.)

In the following, we discuss our results in the context of the directing work of Le et al.⁶². First, our temperature coefficient of the efficiency (TC_η) of $-(0.3 \pm 0.02) \text{ \%}_{\text{rel}}/\text{K}$ is (in absolute numbers) smaller than for PERC ($TC_{\eta,\text{PERC}} = -0.37 \text{ \%}_{\text{rel}}/\text{K}$ ⁷⁶) and only slightly larger than for SHJ ($TC_{\eta,\text{SHJ}} = -0.29 \text{ \%}_{\text{rel}}/\text{K}$ ⁷⁶). The temperature coefficient of the open-circuit voltage $TC_{V_{\text{oc}}} = -(0.25 \pm 0.01) \text{ \%}_{\text{rel}}/\text{K}$ compares to

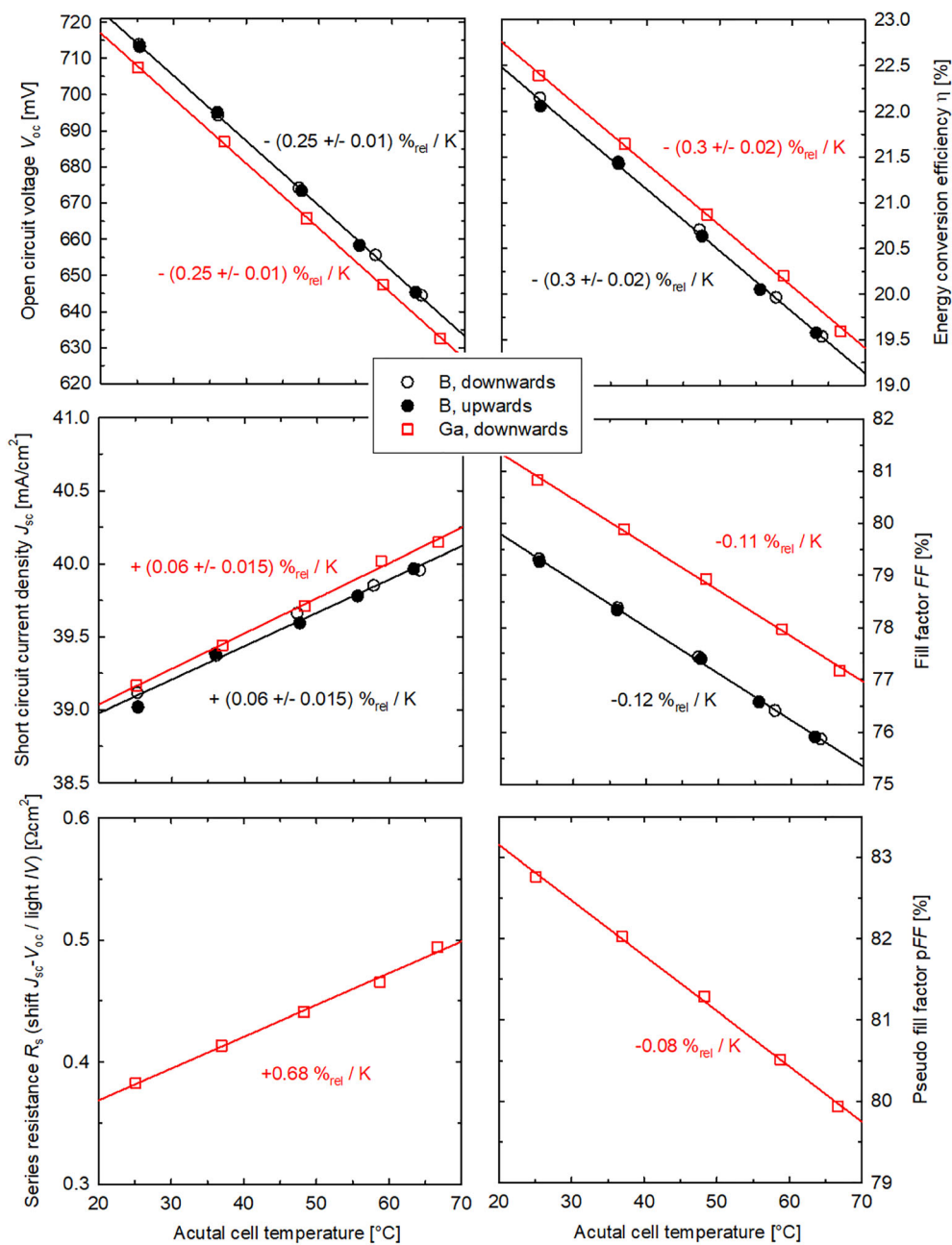


FIGURE 5 Temperature dependency of IV parameters measured on POLO-BJ cells based on either Ga-doped (red) or boron-doped (black) wafers. The cell temperature was first set to the highest value and subsequently decreased (“downwards,” open symbols) or increased starting from 25°C (“upwards,” filled symbols). All measurements were performed in-house on full area (M2) with a busbarless contacting scheme

$TC_{V_{oc,PERC}} = -0.29\%_{rel}/K^{76}$ and is equal to $TC_{V_{oc,SHJ}} = -0.25\%_{rel}/K^{76}$. One should note that these results probably only pose an interim status: If we really succeed in improving V_{oc} from currently 714 mV to the simulated potential of 736 mV, the temperature coefficient of the open-circuit voltage will reduce further (in absolute numbers). When calculating the γ value—as introduced by Green⁷⁷ for the temperature dependency of the diode saturation current density from Equation (2) in Le et al,⁶² we obtain values between 1.1 and 1.5. The temperature coefficient of the short-circuit density $TC_{J_{sc}} = + (0.06 \pm 0.015)\%_{rel}/K$ is larger than of PERC ($TC_{J_{sc,PERC}} = + 0.04\%_{rel}/K^{76}$) and SHJ ($TC_{J_{sc,SHJ}} = + 0.04\%_{rel}/K^{76}$)—which is an advantage in this case. It is interesting to note that our $TC_{J_{sc}}$ value of $+0.06\%_{rel}/K$ is larger than the highest $TC_{J_{sc}}$ value ($TC_{J_{sc,Al-BSF}} = + 0.05\%_{rel}/K^{76}$) of all

technologies compared in the overview of Le et al.⁶² One hypothesis is that both concepts—our POLO-BJ cell and the Al-BSF cell—suffer from optical losses in the infrared regime. In our case, free carrier absorption in the rather thick, highly doped *n*-type poly-Si layer on the rear is significant (0.32 mA/cm^{253}). Since a decrease of the bandgap of the *c*-Si wafer with increasing temperature mostly affects the absorption in the long-wavelength regime, more of this light is absorbed in the wafer before reaching the poly-Si on the rear.

It is particularly interesting to compare the temperature behavior of the *FF* on our cells with the respected behavior on the TOPCon cells on UMG material investigated by Le et al.⁶² These UMG-based TOPCon cells are obviously limited by a strong series resistance ($R_s > 1 \Omega\text{cm}^2$), which is essentially implied by the tunneling-based

poly-Si/SiO_x junction on the rear. Since the tunneling current increases with increasing occupation probability of high energy states in the Si, the series resistance decreases with increasing temperature. This results in an (in absolute numbers) low $TC_{FF, TOPCon, UMG}$ of $-0.07\%_{rel}/K$.⁶² By contrast, our POLO junction scheme—as applied on the POLO-BJ cells—does not contribute significantly to the series resistance. Since pinhole-mediated transport contributes essentially in our junctions, the specific contact resistance even increases with increasing temperature—together with other contributions such as lateral transport of holes in the wafer. Therefore, our temperature coefficient of the fill factor $TC_{FF} = -0.12\%_{rel}/K$ is (in absolute numbers) as large as in PERC cells ($TC_{FF, PERC} = -0.12\%_{rel}/K$ ⁷⁶) with a similar increase in the lateral transport losses with increasing temperature. When considering the temperature behavior of the resistance-free pseudo fill factor, we obtain similar values ($TC_{pFF} = -0.08\%_{rel}/K$) as Le et al. ($TC_{pFF, TOPCon, UMG} = -0.07\%_{rel}/K$).

Eventually, the (in absolute numbers) lower temperature coefficient TC_{FF} of the UMG-based TOPCon cells in Le et al⁶² enables a slightly lower temperature coefficient of the efficiency $TC_{\eta, TOPCon, UMG} = -0.285\%_{rel}/K$ ⁶² than for our POLO-BJ cells. However, we consider the UMG-based TOPCon cells from Le et al⁶² as very specific (due to the high $R_s > 1 \Omega cm^2$ and the moderate STC efficiencies of $\sim 20\%$). Highly efficient TOPCon cells with $\eta >> 20\%$ have a much lower series resistance, probably not limited by the poly-Si/SiO_x junction. An increasing temperature will not relieve a strong limitation—even if the current transport across the poly-Si/SiO_x junction is based on tunneling. Therefore, we think that the temperature coefficient of the efficiency of our cells is comparable to that of TOPCon cells. Both technologies provide an advantage as compared to PERC in this regard.

7 | CONCLUSION AND OUTLOOK

The specific of ISFH's POLO cells is the combination of electron-collecting passivating *n*POLO junctions with conventional Al-alloyed *p*⁺-type regions for hole collection. We use *p*-type Si wafers and implement this concept in front- and back-contacted cell structure with a back junction (POLO-BJ) and in interdigitated back-contacted cell structures (POLO-IBC). Here, we report on the progress for both technologies, in particular on a certified 22.9% efficient POLO BJ cell and a certified 23.7% efficient POLO-IBC cell.

Since these efficiencies—although promising—do not fully exploit the efficiency potential as previously simulated⁵⁰ yet, we perform a simulation-based sensitivity analysis. We focus here on quantities related to the quality of the hole-collecting alloyed Al-*p*⁺ junction—which are subject to continuous improvement and thus hard to predict exactly. The sensitivity analysis shows that the reduction of Al-*p*⁺ recombination and resistance is of high importance for both cell structures. A reduction of J_{0Alp^+} from current values of 600 (830) fA/cm² down to 400 fA/cm² is compatible with a high efficiency potential of 25.4% (24.6%) for POLO-IBC (POLO-BJ). This probably can be reached by adapting the paste ingredients as well as the firing profile.

Therefore, we conclude that the optimization of the quality of the Al-*p*⁺ region is a solvable challenge and not a road blocker. An even better quality of the Al-*p*⁺ region would facilitate even higher efficiencies.

However, the unit cell simulations performed for our sensitivity analysis do not include all loss channels present in our experimental cells. They, in particular, overestimate the fill factor. We, therefore, analyze in detail the recombination-induced pseudo fill factor in our devices. While we measure (implied) pseudo fill factor values up to 85.5% on (even boron-doped) POLO BJ cell precursors prior to metalization, the pseudo fill factor drops on cell level down to 82.9% on POLO-BJ and to 83.9% on POLO-IBC cells. These measured *pFF* values are $\sim 2\%_{abs}$ (POLO-BJ) and $\sim 1\%_{abs}$ (POLO-IBC) lower than the expectations for Ga-doped material at the respective V_{oc} values. We discuss possible root causes for the reduced *pFF*. While further research is required here, it is obvious that an increase of the robustness of the *n*POLO junctions against spiking-through of Ag crystallites and, in the same context, improvement of the quality of the Al-*p*⁺ regions by an increase of the firing temperature is desirable. For this purpose, we propose the concept of an embedded blocking layer for the Ag crystallites in the poly-Si—ideally realized in situ during the Si deposition. While an evaluation of this concept on cell level is still ongoing and thus future publications have to report on the results, the concept of the EBL is one example of how the limitations described above could be addressed.

Since there probably are further solutions, we are confident that our current results only pose an interim status. Indeed, our learning rate is quite steep with $\sim 1\%_{abs}$ improvement per year⁵⁹—despite our (compared to a pilot line) rather limited throughput and long feedback time. We, therefore, think that both the POLO-BJ and the POLO-IBC technology can be optimized to efficiencies of $>24.5\%$ and $>25\%$ on midterm.

Besides the efficiency improvement, we are working on the elaboration of further positive aspects of our technology. One aspect in this regard are concepts for further material cost reduction such as the “all-Al” POLO-BJ cell⁵⁹—which would be also applicable to the POLO-IBC structure. Another aspect is that the rather high open-circuit voltages of our cells also result in an (in absolute numbers) reduced temperature coefficient. We report here on our first evaluation of the temperature behavior, resulting in a temperature coefficient for the efficiency of $-(0.3 \pm 0.02)\%_{rel}/K$ for POLO-BJ cells on boron and Ga-doped material. This compares to a $TC_{\eta, PERC}$ of $-0.37\%_{rel}/K$.⁷⁶ An analysis of the temperature dependence of all *IV* parameters, in particular of the contributions to the fill factor, reveals distinct differences between our cells and tunneling resistance-limited TOPCon cells from Le et al.⁶²

As an outlook toward future development steps of the ISFH roadmap,⁵⁰ we mention that both our POLO-BJ and our POLO-IBC cells can be modified to become two-terminal⁷⁸ or three-terminal⁷⁹ bottom cells, bridging from PERC to Si-based tandem.⁷⁸ The two-terminal perovskite-POLO-PERC+ tandem (“P³T”) concept has been positively assessed cost-wise.⁸⁰ We recently presented a first two-terminal proof-of-concept device.⁸¹

ACKNOWLEDGEMENTS

We would like to thank Anja Christ, Annika Raugewitz, Hilke Fischer, Magalie Pollmann, Renate Winter, Bianca Gehring, and Thomas Friedrich for sample processing and David Sylla and Tobias Neubert for laser structuring and *I*-*V* measurements. We furthermore would like to thank David Hinken, Dominic Walter, and Michael Rienäcker for valuable discussions. Also, we would like to thank Raymond Zieseniß, Guido Glowatzki and Jan Krügener from the Institute for Electronic Materials and Devices of the Leibniz University Hannover for the excellent cooperation and the supply of LPCVD-based poly-Si layers.

We also thank TOYO Aluminium for providing the Al-paste, Heraeus and Dupont, for providing the Ag-pastes, and Longi for providing the wafer material.

This work was funded by the German Federal Ministry for Economic Affairs and Energy (BMWi) under contact number 0324275A (Street) and contact number 03EE1012A (NanoPERC), as well as by the state of Lower Saxony.⁴¹

Open Access funding enabled and organized by Projekt DEAL.

DATA AVAILABILITY STATEMENT

The data that support the findings of this study are available from the corresponding author upon reasonable request.

ORCID

Robby Peibst  <https://orcid.org/0000-0001-8769-9392>

ENDNOTES

* One should note that the original motivation of the pinhole model¹⁴ was the symmetric electrical behavior of electron- and hole-collecting n-type of p-type doped poly-Si/SiO_x junctions, which seems to pose-independent from the oxide thickness—an inconsistency of the tunneling model with higher energy barriers for holes than for electrons.

† In this work, we use the abbreviation “TOPCon” as denotation of the specific cell structure rather than for the denotation of the junction scheme.

‡ An analysis of the series resistance of our cells is beyond the scope of this paper. The total values of $\sim 0.38 \Omega\text{cm}^2$ ($\sim 0.48 \Omega\text{cm}^2$) for POLO-BJ (POLO-IBC) are not extremely high and can be decomposed straight forward into the single contributions. Besides the contribution from the metal grid ($\sim 0.2 \Omega\text{cm}^2$ for POLO-IBC), all contributions are included in the unit cell simulations.

§ We would like to remark that, unless one does not target also Ag-free cell interconnection concepts like foil-based Al laser welding, one still needs Ag soldering pads. Although the Ag consumption would still be reduced significantly in this case, the term “all-Al cell”—while catchy and easy to understand—would not be accurate.

REFERENCES

- Takagi M, Nakayama K, Tevada C, Kamioko H. Improvement of shallow base transistor technology by using a doped polysilicon diffusion source. *The Journal of the Japan Society of Applied Physics*. 1972;42:101-109.
- Graul J, Glasl A, Murrmann H. High-performance transistors with arsenic implanted polysil emitters. *IEEE Journal of Solid-State Circuits*. 1976;11(4):491-495.
- Lieblich Z, Bar-Lev A. A polysilicon-silicon n-p junction. *IEEE Transactions on Electron Devices*. 1977;24(8):1025-1031.
- Fossum J, Shibib M. A minority-carrier transport model for polysilicon contacts to silicon bipolar devices, including solar cells. *Ire*. 1980;280-283.
- Lindholm F, Neugroschel A, Arienzo M, Iles P. Heavily doped polysilicon-contact solar cells. *IEEE Electron Device Letters*. 1985;6(7):363-365.
- Sah C. High efficiency crystalline silicon solar cells. *Solar Cells*. 1986;17(1):1-27.
- Yablonovitch E, Gmitter T, Swanson RM, Kwark YH. A 720 mV open circuit voltage SiO_x:c-Si:SiO_x double heterostructure solar cell. *Appl Phys Lett*. 1985;47(11):1211-1213.
- Tarr N. A polysilicon emitter solar cell. *IEEE Electron Device Letters*. 1985;6(12):655-658.
- Castaner L. Effects of fluorine in silicon solar cells with polysilicon contacts. *Solar Energy Materials and Solar Cells*. 1998;53(1-2):115-129.
- Brendel R, Dullweber T, Gogolin R, et al. Recent progress and options for future crystalline silicon solar cells. In Proceedings of the 28th European Photovoltaic Solar Energy Conference and Exhibition, WIP, Paris, France, pp. 676-690. 2013.
- Feldmann F, Bivour M, Reichel C, Hermle M, Glunz SW. A passivated rear contact for high-efficiency n-type Si solar cells enabling high Voc's and FF>82%. In Proceedings of the 28th European Photovoltaic Solar Energy Conference and Exhibition, WIP, Paris, France, pp. 988-992. 2013.
- Römer U, Peibst R, Lim B, et al. Recombination behaviour and contact resistance of n+ and p+ polycrystalline Si/monocrystalline Si junctions. *Solar Energy Materials and Solar Cells*. 2014;131:85-91.
- Römer U, Peibst R, Ohrdes T, et al. Ion implantation for poly-Si passivated back-junction back-contacted solar cells. *IEEE Journal of Photovoltaics*. 2015;5(2):507-514.
- Peibst R, Römer U, Hofmann KR, et al. A simple model describing the symmetric IV characteristics of p polycrystalline Si/n monocrystalline Si and n polycrystalline Si/p monocrystalline Si junctions. *IEEE Journal of Photovoltaics*. 2014;4(3):841-850.
- Peibst R, Römer U, Larionova Y, et al. Working principle of carrier selective poly-Si/c-Si junctions: Is tunnelling the whole story? *Solar Energy Materials and Solar Cells*. 2016;158:60-67.
- Tetzlaff D, Krügener J, Larionova Y, et al. Evolution of oxide disruptions: the (w)hole story about passivating contacts. IEEE 43rd Photovoltaic Specialists Conference (PVSC), 0221-0224, Portland, OR, USA. 2016.
- Guthrey H, Salles CL, Kale AS, et al. Effect of surface texture on pinhole formation in SiO_x-based passivated contacts for high-performance silicon solar cells. *ACS Appl Mater Interfaces*. 2020;12(50):55737-55745.
- Tetzlaff D, Krügener J, Larionova Y, et al. A simple method for pinhole detection in carrier selective POLO-junctions for high efficiency silicon solar cells. *Solar Energy Materials and Solar Cells*. 2017;173:106-110.
- Wietler TF, Tetzlaff D, Krügener J, et al. Pinhole density and contact resistivity of carrier selective junctions with polycrystalline silicon on oxide. *Appl Phys Lett*. 2017;110(25):253902.
- Kale AS, Nemeth W, Guthrey H, et al. Understanding the charge transport mechanisms through ultrathin SiO_x layers in passivated contacts for high-efficiency silicon solar cells. *Appl Phys Lett*. 2019;114(8):083902.
- Feldmann F, Nogay G, Löper P, et al. Charge carrier transport mechanisms of passivating contacts studied by temperature-dependent J-V measurements. *Solar Energy Materials and Solar Cells*. 2018;178:15-19.
- Folchert N, Rienäcker M, Yeo AA, Min B, Peibst R, Brendel R. Temperature-dependent contact resistance of carrier selective poly-Si on oxide junctions. *Solar Energy Materials and Solar Cells*. 2018;185:425-430.

23. Galleni L, Firat M, Sivaramakrishnan Radhakrishnan H, Duerinckx F, Tous L, Poortmans J. Mechanisms of charge carrier transport in polycrystalline silicon passivating contacts. *Solar Energy Materials and Solar Cells*. 2021;232:111359.
24. Bayerl P, Folchert N, Bayer J, et al. Contacting a single nanometer-sized pinhole in the interfacial oxide of a poly-silicon on oxide (POLO) solar cell junction. *Progress in Photovoltaics: Research and Applications*. 2021;29(8):936-942.
25. Folchert N, Peibst R, Brendel R. Modeling recombination and contact resistance of poly-Si junctions. *Progress in Photovoltaics: Research and Applications*. 2020;28(12):1289-1307.
26. Cuevas A, Yan D. Misconceptions and misnomers in solar cells. *IEEE Journal of Photovoltaics*. 2013;3(2):916-923.
27. Haase F, Hollemann C, Schäfer S, et al. Laser contact openings for local poly-Si-metal contacts enabling 26.1%-efficient POLO-IBC solar cells. *Solar Energy Materials and Solar Cells*. 2018;186:184-193.
28. Richter A, Müller R, Benick J, et al. Design rules for high-efficiency both-sides-contacted silicon solar cells with balanced charge carrier transport and recombination losses. *Nat Energy*. 2021;6(4):429-438.
29. Stodolny MK, Lenes M, Wu Y, et al. N-type polysilicon passivating contact for industrial bifacial n-type solar cells. *Solar Energy Materials and Solar Cells*. 2016;158:24-28.
30. Tao Y, Upadhyaya V, Chen C-W, et al. Large area tunnel oxide passivated rear contact n-type Si solar cells with 21.2% efficiency. *Prog Photovolt: Res Appl*. 2016;24(6):830-835.
31. Duttagupta S, Nandakumar N, Padhamnath P, Kitz Buatis J, Stangl R, Aberle AG. monoPoly™ cells: large-area crystalline silicon solar cells with fire-through screen printed contact to doped polysilicon surfaces. *Solar Energy Materials and Solar Cells*. 2018;187:76-81.
32. Chen D, Chen Y, Wang Z, et al. 24.58% total area efficiency of screen-printed, large area industrial silicon solar cells with the tunnel oxide passivated contacts (i-TOPCon) design. *Solar Energy Materials and Solar Cells*. 2020;206:110258.
33. Press release from Longi Solar from June 2nd 2021. <https://www.pv-magazine.com/2021/06/02/longi-achieves-25-21-efficiency-for-topcon-solar-cell-announces-two-more-records/>
34. Press release from Jinko Solar from Oct. 14th 2021. <https://www.pv-tech.org/jinkosolar-claims-new-record-taking-n-type-cell-conversion-efficiency-to-25-4/>
35. Green MA, Dunlop ED, Hohl-Ebinger J, Yoshita M, Kopidakis N, Hao X. Solar cell efficiency tables (version 58). *Prog Photovolt Res Appl*. 2021;29(7):657-667.
36. Press release from Hanwha Q. Cells from Sep. 13th 2021. <https://www.pv-magazine.com/2021/09/13/hanwha-q-cells-unveils-plan-to-produce-perovskite-topcon-solar-modules/>
37. <https://www.pv-tech.org/longi-launches-maiden-n-type-module-featuring-570w-output-and-22-3-efficiency/>
38. Kang D, Sio HC, Yan D, Stuckelberger J, Liu R, Macdonald D. Firing stability of doped polysilicon passivation layers. Proc. of the 37th European Photovoltaic Solar Energy Conference and Exhibition, pp 188-192. 2020.
39. van de Loo, Macco B, Schnabel M, et al. On the hydrogenation of Poly-Si passivating contacts by Al₂O₃ and SiN thin films. *Sol Energy Mater sol Cell*. 2020;215:110592.
40. Steinhäuser B, Feldmann F, Ourinson D, Nagel H, Fellmeth T, Hermle M. On the influence of the SiN_x composition on the firing stability of poly-Si/SiN_x stacks. *Phys Stat Sol*. 2020;217(21):2000333.
41. Hollemann C, Folchert N, Harvey SP, Stradins P, Young DL. Changes in hydrogen concentration and defect state density at the poly-Si/SiO_x/c-Si interface due to firing. *Solar Energy Materials and Solar Cells*. 2021;231:111297.
42. Hollemann C, Rienäcker M, Soeriyadi A, et al. Firing stability of tube furnace-annealed n-type poly-Si on oxide junctions. *Prog Photovolt Res Appl*. 2021;30(1):1-16.
43. Çiftçinar HE, Stodolny MK, Wu Y, et al. Study of screen printed metallization for polysilicon based passivating contacts. *Energy Procedia* 124. 2017;124:851-861.
44. Padhamnath P, Khanna A, Balaji N, et al. Progress in screen-printed metallization of industrial solar cells with SiO_x/poly-Si passivating contacts. *Solar Energy Materials and Solar Cells*. 2020;218:110751.
45. Press release from Jinko Solar, June 24th (2021), <https://www.pv-tech.org/topcon-presents-immediate-n-type-advantages-as-jinkosolar-keeps-ibc-tandem-cells-on-its-rd-radar/>
46. Smith DD, Cousins P, Westerberg S, Jesus-Tabajonda RD, Aniero G, Shen Y. Toward the practical limits of silicon solar cells. *IEEE Journal of Photovoltaics*. 2014;4(6):1465-1469.
47. <https://www.pv-tech.org/lg-electronics-neon-r-solar-panel-has-365-watt-rating-with-improved-tempera/>
48. Brendel R, Kruse C, Merkle A, Schulte-Huxel H, Haase F, Peibst R. Screening carrier selective contact combinations for novel crystalline Si cell structures. Proc. of the 35th European Photovoltaic Solar Energy Conference and Exhibition, pp. 39-46. 2018.
49. Schmidt J, Peibst R, Brendel R. Surface passivation of crystalline silicon solar cells: present and future. *Solar Energy Materials and Solar Cells*. 2018;187:39-54.
50. Kruse CN, Schäfer S, Haase F, et al. Simulation-based roadmap for the integration of poly-silicon on oxide contacts into screen-printed crystalline silicon solar cells. *Sci Rep*. 2021;11(1):996.
51. Dullweber T, Kranz C, Peibst R, et al. PERC+: industrial PERC solar cells with rear Al grid enabling bifaciality and reduced Al paste consumption. *Progress in Photovoltaics: Research and Applications*. 2016; 24(12):1487-1498.
52. Dullweber T, Schmidt J. Industrial silicon solar cells applying the passivated emitter and rear cell (PERC) concept - a review. *IEEE Journal of Photovoltaics*. 2016;6(5):1366-1381.
53. Min B, Wehmeier N, Brendemuehl T, et al. A 22.3% efficient p-type back junction solar cell with an Al-printed front-side grid and a passivating n+-type polysilicon on oxide contact at the rear side. *Solar RRL*. 2020;4(12):2000435.
54. Min B, Wehmeier N, Brendemuehl T, et al. 716 mV open-circuit voltage with fully screen-printed p-type back junction solar cells featuring an aluminum front grid and a passivating polysilicon on oxide contact at the rear side. *Solar RRL*. 2021;5(1):2000703.
55. Bende EE. Metallization and Interconnection Workshop. 2017.
56. Haase F, Hollemann C, Schaefer S, Kruegener J, Brendel R, Peibst R. Transferring the record p-type Si POLO-IBC cell technology towards an industrial level. 2019.
57. Haase F, Min B, Hollemann C, Krügener J, Brendel R, Peibst R. Fully screen-printed silicon solar cells with local Al-p+ and n-type POLO interdigitated back contacts with a VOC of 716 mV and an efficiency of 23%. *Progress in Photovoltaics: Research and Applications*. 2021; 29(5):516-523.
58. Peibst R. Still in the game. *Nat Energy*. 2021;6(4):333-334.
59. Min B, Wehmeier N, Schulte-Huxel H, et al. Approaching 23% with p-type back junction solar cells featuring screen-printed Al front grid and passivating rear contacts. Proc. of the 38th European Photovoltaic Solar Energy Conference and Exhibition. 2021.
60. Haase F, Hollemann C, Wehmeier N, et al. 23%-efficient screen-printed IBC cells on Cz-grown silicon with n-type poly-Si passivating contact and Al-alloyed p-type contact. Presented at the SiliconPV 2021. 2021.
61. Dullweber T, Stöhr M, Kruse C, et al. Evolutionary PERC+ solar cell efficiency projection towards 24% evaluating shadow-mask-deposited poly-Si fingers below the Ag front contact as next improvement step. *Solar Energy Materials and Solar Cells*. 2020;212:110586.
62. Le AHT, Basnet R, Yan D, et al. Temperature-dependent performance of silicon solar cells with polysilicon passivating contacts. *Solar Energy Materials and Solar Cells*. 2021;225:111020.

63. Fell A. A free and fast three-dimensional/two-dimensional solar cell simulator featuring conductive boundary and quasi-neutrality approximations. *IEEE Trans Electron Dev.* 2013;60(2):733-738.
64. Basore P. <https://www.pc3d.info/>. Accessed on March 23, 2021.
65. Bao J, Chen C, Ma L, et al. Towards 24% efficiency for industrial n-type bifacial passivating-contact solar cells with homogeneous emitter. Proc. of the 37th European Photovoltaic Solar Energy Conference and Exhibition, pp. 160-163. 2020.
66. Brendel R. Modeling solar cells with the dopant-diffused layers treated as conductive boundaries. *Prog Photovolt: Res Appl.* 2012; 20(1):31-43.
67. McIntosh KR, Black LE. On effective surface recombination parameters. *J Appl Phys.* 2014;116(1):014503.
68. Hollemann C, Haase F, Schäfer S, Krügener J, Brendel R, Peibst R. 26.1%-efficient POLO-IBC cells: quantification of electrical and optical loss mechanisms. *Progress in Photovoltaics: Research and Applications.* 2019;27(11):950-958.
69. Breitenstein O, Altermatt P, Ramspeck K, Green MA, Zhao J, Schenk A. Interpretation of the commonly observed I-V characteristics of c-Si cells having ideality factor larger than two. 2006 IEEE 4th World Conference on Photovoltaic Energy Conference, pp. 879-884. 2006.
70. Press release from Longi solar from Oct. 29th 2021. <https://www.pv-magazine.com/2021/10/29/longi-improves-efficiency-of-its-heterojunction-cell-from-25-82-to-26-30-in-just-one-week/>
71. Richter A, Glunz SW, Werner F, Schmidt J, Cuevas A. Improved quantitative description of Auger recombination in crystalline silicon. *Phys Rev B Condens Matter.* 2012;86(16):165202.
72. Walter D, Lim B, Schmidt J. Realistic efficiency potential of next-generation industrial Czochralski-grown silicon solar cells after deactivation of the boron-oxygen-related defect center. *Progress in Photovoltaics: Research and Applications.* 2016;24(7):920-928.
73. Lim B, Merkle A, Peibst R, Dullweber T, Wang Y, Zhou R. LID-free PERC+ solar cells with stable efficiencies up to 22.1%. Proc of the 35th European Photovoltaic Solar Energy Conference and Exhibition, pp. 359-365. 2018.
74. Haase F, Schäfer S, Klamt C, et al. Perimeter recombination in 25%-efficient IBC solar cells with passivating POLO contacts for both polarities. *IEEE Journal of Photovoltaics.* 2018;8(1):23-29.
75. Min B, Müller M, Wolpensinger B, et al. Impact of local back-surface-field thickness variation on performance of PERC solar cells. *IEEE Journal of Photovoltaics.* 2021;11(4):908-913.
76. Haschke J, Seif JP, Riesen Y, et al. The impact of silicon solar cell architecture and cell interconnection on energy yield in hot & sunny climates. *Energ Environ Sci.* 2017;10(5):1196-1206.
77. Green MA. *Solar Cells: Operating Principles, Technology, and System Applications.* Prentice-Hall; 1982.
78. Peibst R, Rienäcker M, Min B, et al. From PERC to tandem: POLO- and p+/n+ poly-Si tunneling junction as interface between bottom and top cell. *IEEE Journal of Photovoltaics.* 2019;9(1):49-54.
79. Rienäcker M, Warren EL, Wietler TF, Tamboli AC, Peibst R. Three-terminal bipolar junction bottom cell as simple as PERC: towards lean tandem cell processing. Proc of the 46th IEEE Photovoltaic Specialist Conference (PVSC). 2019.
80. Messmer C, Goraya BS, Nold S, et al. The race for the best silicon bottom cell: efficiency and cost evaluation of perovskite-silicon tandem solar cells. *Prog Photovolt Res Appl.* 2021;29(7):744-759.
81. Peibst R, Haase F, Hollemann C, et al. Exploiting single junction efficiency potentials and going beyond. Presented at the 38th EUPVSEC. 2021.

How to cite this article: Peibst R, Haase F, Min B, et al. On the chances and challenges of combining electron-collecting nPOLO and hole-collecting Al-p⁺ contacts in highly efficient p-type c-Si solar cells. *Prog Photovolt Res Appl.* 2023;31(4): 327-340. doi:10.1002/pip.3545